RSC Advances

PAPER

View Article Online
View Journal | View Issue

Cite this: *RSC Adv.*, 2026, **16**, 23167

Sustainable green-synthesized hematite nanocatalysts and their efficient reduction of aromatic nitro pollutants

Johnson Paul Jesudasson,[a] Monikadevi P.,[a] Rama P.,[a] Jothika M.,[a] Sivakami S.,[a] Selvaraj Mohana Roopan[b] and Karuppiah Muthu *[a]

Aromatic nitro compounds (ANCs) are extremely harmful environmental pollutants that cause severe threats to the environment and human life. This is why the development of effective and non-polluting methods for their elimination is extremely significant. In this study, hematite nanoparticles (HNPs) were prepared using a green and eco-friendly method involving the leaf extract of *Sesbania grandiflora*. The extract of the plant acted as a reducing and stabilizing agent in the formation of the nanoparticles, making it a cost-effective and sustainable synthesis pathway. The obtained HNPs were identified by UV-vis spectroscopy, FTIR spectroscopy, PXRD, HRTEM and EDAX analysis to ascertain the structural and morphological characteristics of the synthesized nanoparticles. The prepared HNPs were tested as catalysts towards the reduction of different aromatic nitro compounds. Kinetic measurements showed that the reduction followed pseudo-first-order kinetics and that mono-nitro compounds reduced much faster in this system than in traditional reduction systems. Moreover, the catalyst was very stable and recyclable and could sustain high catalytic activity for up to six consecutive reaction cycles. The results prove that green-synthesized HNPs can act as effective nanocatalysts for the removal of nitroaromatic pollutants from contaminated water systems.

Received 23rd December 2025
Accepted 21st April 2026

DOI: 10.1039/d5ra09934j

rsc.li/rsc-advances

1 Introduction

In the modern era, water pollution has garnered considerable attention, primarily owing to the presence of various pollutants, including heavy metal ions, pesticides, dyes, plastics, and nitroaromatic compounds.[1] Among all these harmful pollutants, nitroaromatic compounds have emerged as a considerable source of contamination.[2] Nitroarenes are introduced into the environment through various routes, mainly from petroleum products and fumes released during their combustion.[3] In particular, chemicals like TNT, manufactured for military purposes, play a major role in environmental pollution.[4] Due to the persistence and toxic nature of aromatic nitro compounds (ANCs), they pose a threat because of their mutagenic and carcinogenic activities,[2] which may have adverse impacts on wildlife[3] and human health.[3] The challenge posed by water pollution requires efficient approaches for transforming harmful nitro compounds (NC) into amine derivatives.[5] Aromatic amines, as products of this transformation, play a significant role in different industries, including the dye, polymer, biochemical, pharmaceutical, and pesticide industries.[6] Hence, it can be concluded that the search for remediation methods for nitroarene-contaminated water also offers prospects for exploring new industrial applications.[7] The varying challenge in water pollution due to nitro derivative substances highlights the need for research and innovative inputs in finding measures to effectively combat this menace.[8] By concentrating efforts on modifying noxious substances such as NCs into valuable amines, we can look forward to a cleaner and less hazardous environment while exploiting the advantages of these amines in various applications.[9]

A highly efficient method of transforming NCs into amines in an aqueous medium is to use catalysts and reducing agents.[10] However, the conventional routes of transforming NCs into amines using reducing agents and catalysts face many challenges. Over the years, such routes have been characterized by disadvantages such as toxicity, high cost, recyclability, and the occurrence of poisoning effects.[11] A more promising alternative in the conversion of NCs to amines is the use of metal nanoparticles (MNPs) or metal oxide nanoparticles (MONPs).[12] It has been further noted that MNPs and MONPs, composed of noble metals including Au, Ag, Pt, and Pd, display remarkable efficiency in catalytic reactions.[13] However, due to the high cost involved in synthesizing these NPs, cheaper materials have been sought. Some of the most efficient materials include 3-d transition MNPs. Not only is the cost of the materials significantly

[a]*Department of Chemistry, Manonmaniam Sundaranar University, Abishekapatti, Tirunelveli 627012, Tamil Nadu, India. E-mail: karu.muthu@msuniv.ac.in*
[b]*Department of Chemistry, Chemistry of Heterocycles and Natural Product Research Laboratory, School of Advanced Sciences, Vellore Institute of Technology, Vellore 632014, Tamil Nadu, India*

low but also these materials display high efficiency in catalysis.[14] The use of these materials and MONPs may greatly reduce the volume of solvents involved in the catalytic conversion of NC, an important consideration for sustainability.[15] Despite the variety of techniques that exist to synthesize MNPs and MONPs, one of the most efficient synthesis routes is offered by green synthesis, which impacts very positively on environmental remediation.[16] Among the 3-d transition metals, there is strong industry-driven interest in determining which type of catalyst is most effective. Among the most efficient types of selective transformation catalysts is the iron (Fe) based one. The synthesis of Fe particles produces a selective transformation catalyst best utilized within a series of organic transformations such as hydrogenation, the hydrogen transfer reaction, and the C–C coupling reaction.[17–19]

The use of a plant extract as a method in green synthesis can be thought of as exemplary, with plant extracts existing in a dual capacity as both capping and reducing agents.[20] The responsible phytocompounds in the plant extracts mainly include carbonyl (–C═O) and hydroxyl (–OH) groups, giving them the dual capacity.[21,22] This greatly reduces the cost involved when synthesizing MNPs and MONPs.[23] The green approach, though carrying much impact, has certain minor disadvantages, like seasonal collection of plant materials, processes being lengthy, and variations in particle size depending on the phytochemical composition present in the plant extract. Such considerations remain important in the application of sustainable practice measures.[24] However, this approach can be balanced for the fabrication process. A major step forward in enhancing the progress of nitro to amine conversion reactions using MNP and MONP, especially in regard to more eco-friendly synthesis methods, appears to show promise in terms of enhanced catalytic efficiency and cost-effectiveness.[25] This analysis has also been able to show the prospects offered by green chemistry in terms of promoting sustainability in chemical reactions.[26]

Sesbania grandiflora is a widely available plant rich in bioactive compounds such as tannins, carbohydrates, proteins, and alkaloids. These phytochemicals play an important role in the formation and stabilization of nanoparticles during green synthesis. In the present study, hematite nanoparticles (HNPs) were synthesized using the leaf extract of *S. grandiflora* through a simple green synthesis approach. The catalytic efficiency of the synthesized HNPs was evaluated for the reduction of various aromatic nitro compounds. In addition, the recyclability and catalytic stability of the nanoparticles were systematically investigated to assess their potential applications in environmental remediation.

2 Materials and methods

2.1 Materials

All chemicals used in this study were of analytical reagent (AR) grade and used without further purification. Ferrous sulphate heptahydrate ($FeSO_4 \cdot 7H_2O$, 98%), sodium borohydride ($NaBH_4$, 98%), and sodium hydroxide pellets (NaOH, 97%) were purchased from SRL Pvt. Ltd (India). The aromatic nitro compounds used in this study included 4-nitrophenol (4-NP, 98%), 2-nitrobenzaldehyde (2-NB, 99%), 4-nitroaniline (4-NA, 98%), and 2,4-dinitroaniline (2,4-DNA, 98%).

2.2 Aqueous extract of *S. grandiflora* leaf extract

The *S. grandiflora* samples were fresh leaves collected at Nanjankulam, Tirunelveli, Tamil Nadu, India. The harvested leaves were rinsed under running tap water then under deionized water to remove dust and impurities. The leaves were dried overnight at a temperature of 30 °C. About 70 g of dried leaves were cut into small sizes and moved to the reaction vessel with 400 mL of triple-distilled water. The mixture was refluxed over 30 min to harvest the phytochemical compounds. After refluxing, the extract was filtered through Whatman No. 1 filter paper to remove plant residues. The resulting filtrate was kept at 4 °C to be used later in the preparation of nanoparticles.[27]

2.3 Synthesis of HNPs

The synthesis of HNPs was done by co-precipitation. First, 2.78 g of $FeSO_4 \cdot 7H_2O$ (0.1 M) was dissolved in 100 mL of triple-distilled water. A 50 mL volume of this solution was added to a conical flask and stirred magnetically at 60 °C for 1 h. Then, 15 mL of *S. grandiflora* leaf extract was added to the reaction mixture with continuous stirring.[28–30] The color was observed to rapidly change to brown after a few minutes, which implied the creation of nanoparticles. Then, 10 mL of 1 M NaOH solution was gradually added to the solution, and the reaction was maintained for at least an hour more to allow total precipitation. The reaction mixture was left overnight in the dark at room temperature. Centrifugation was used to collect the precipitate, which was washed with triple-distilled water several times in order to eliminate impurities. The pure hematite nanoparticle product was eventually obtained by drying and calcining the obtained product in a muffle furnace at 500 °C for 4 h.

2.4 Characterization techniques

A set of sophisticated methods of analysis was used to systematically characterize the synthesized HNPs in terms of their structural, optical and morphological characteristics. UV-visible spectroscopy (PerkinElmer Lambda 25) was performed to determine the absorbance spectrum in the wavelength range of 200–800 nm. A SHIMADZU IR Tracer-100 spectrometer was used at the wavelengths of 4000–400 cm^{-1} with the KBr pellet technique to conduct Fourier transform infrared (FTIR) spectroscopy. This was analyzed to determine the functional groups and molecular vibration of the synthesized HNPs as well as to establish their chemical composition. X-ray diffraction (XRD) served to determine the crystalline structure and phase purity of the product using a Bruker ECO D8 ADVANCE diffractometer. The diffraction patterns were documented within the 2–70° 2 theta range to determine crystallinity and structural parameters. High-resolution transmission electron microscopy (HRTEM) was employed to discover the surface morphology, particle size, and microstructure of the HNPs with a JEOL JEM-2100 Plus instrument (JEOL, Japan). Using this method, the morphology of the particles and their size distribution were observed in a detailed manner. The textural properties,

including surface area and pore diameter, were assessed by using an Anton Paar Quantachrome Autosorb iQ surface area analyzer.

2.5 Reduction of ANC

The study of the reduction kinetics of HNPs was carried out using different ANCs, such as 4-NP, 2-NB, 4-NA, and 2,4-DNA. Initially, 1 M solutions of different ANCs were prepared in 50 mL of SMF using TDW. At the same time, 1 M solutions of $NaBH_4$ were prepared in 10 mL of SMF. The initial stage of the study was centred on evaluating different mol% of HNPs equivalent to ANC in order to determine optimal conditions for achieving the maximum reduction conversion percentage at room temperature (38 °C). The major kinetic effort in this paper was the reduction of ANC with HNPs compared to the reduction kinetics of ANC by $NaBH_4$ under similar ambient conditions. Time-dependent methods were employed for 10 minutes to evaluate the efficacy of the reductions. Besides these efforts, this study researched the reusability of HNPs and their continued reduction activity on ANC, with a focus on the pragmatic applications of these materials in environmental remediation and chemical synthesis. This comprehensive investigation provides valuable insights into the effectiveness of HNPs in catalytic reduction processes, pointing out their potential applications in various chemical transformations.

3 Result and discussion

3.1 Characterization of HNPs

Primarily, the synthesis of HNPs performed with *S. grandiflora* was validated by the color change from yellow to brown within 2 min. This change in color, which is quite rapid, manifests a clear indication of the synthesis taking place. The UV-visible absorption spectrum of the synthesized HNPs is presented in Fig. 1a. The spectrum exhibits characteristic absorption bands at approximately 207 nm, 332 nm, and 382 nm, indicating the formation of iron oxide nanoparticles. The absorption band observed around 207 nm can be attributed to Fe–O charge transfer transitions within the iron oxide lattice. The additional absorption peaks at 332 nm and 382 nm are associated with electronic transitions related to Fe–O bonds in the hematite structure. These absorption features arise due to electronic

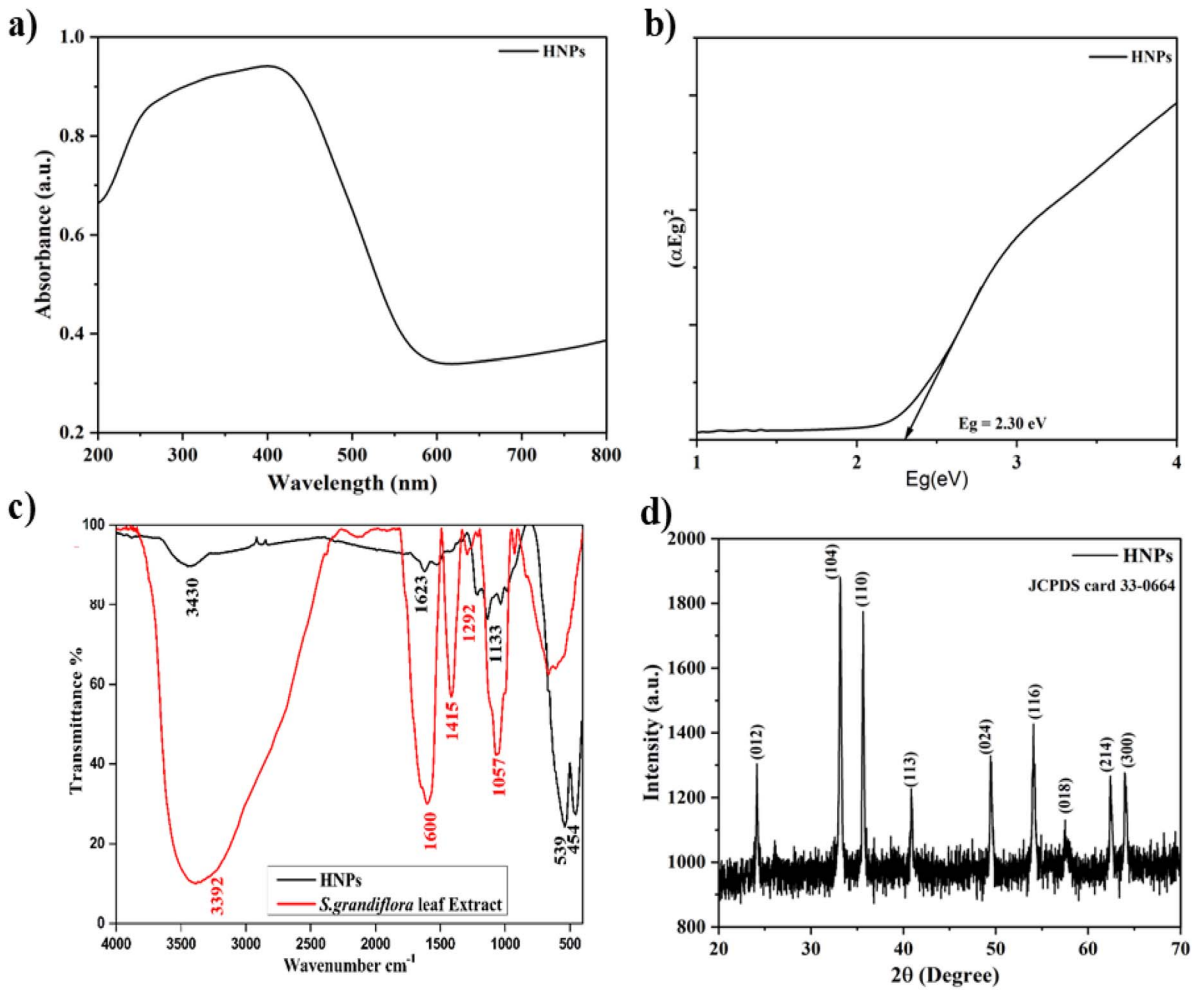

Fig. 1 Eco-friendly HNPs synthesized using the *S. grandiflora* leaf extract: (a) UV-vis absorbance spectrum; (b) band gap using Tauc plot; (c) FTIR analysis; and (d) PXRD analysis.

excitation from the valence band to the conduction band of the semiconductor material. Furthermore, the optical band gap of the synthesized HNPs was estimated using the Tauc plot method, as illustrated in Fig. 1b. The calculated band gap value was found to be approximately 2.1 eV, which is consistent with previously reported values for HNPs.[31,32]

The functional groups found in the leaf extract of *S. grandiflora* as well as in the synthesized HNPs were studied thoroughly using FTIR spectroscopy, as depicted in Fig. 1c. Analysis of the FTIR spectrum of the leaf extract of *S. grandiflora* revealed the presence of particular bands around 3392, 1600, 1415, 1292, and 1057 cm^{-1}. On the other hand, the FTIR spectrum of the HNPs possessed bands around 3430, 1623, 1133, 539, and 454 cm^{-1}. Observation of the spectrum of the leaf extract confirmed that the broad peak observed around 3392 cm^{-1} is attributable to the –OH stretching frequency of alcohol functional groups. Furthermore, the appearance of the band at 1600 cm^{-1} indicates C=O stretching, which is typical of carbonyl groups. In addition, the peak present at 1415 cm^{-1} is due to the –OH bending of the alcohol group. Moreover, the C–N stretching of an amine group is indicated by the band at 1292 cm^{-1}. The peak attributed to the C–O–C stretching vibration of an ester functional group is present at 1057 cm^{-1}. Furthermore, the FTIR spectrum of the HNPs indicates the existence of a characteristic peak at 3430 cm^{-1} related to the –OH stretching group. Significantly, the peaks at 539 and 454 cm^{-1} are indicative of the Fe–O stretching band,[33] which is crucial for confirming the evidence of iron oxide in the NPs. The –OH and C=O functional groups serve as both reducing and stabilizing (capping) agents during the synthesis of HNPs. This was clearly identified by the decrease in transmittance, which suggests that the HNPs were formed through the interaction of the carbonyl and alcohol functional groups in the *S. grandiflora* leaf extract. Furthermore, the absorption bands observed at 539 cm^{-1} and 454 cm^{-1} correspond to Fe–O stretching vibrations, confirming the formation of iron oxide nanoparticles. From this FTIR spectrum, we can confirm that phytocompounds such as tannins, proteins, carbohydrates and alkaloids were present in the *S. grandiflora* leaf extract.[29]

An XRD analysis of the HNPs was meticulously performed utilizing Cu-Kα radiation, as depicted in Fig. 1c. The examination showed clear peak values that matched the 2θ angles at 24.13°, 33.15°, 35.62°, 40.86°, 49.45°, 54.08°, 57.55°, 62.45°, and 64.04°. These peaks were associated with their respective Miller indices as (012), (104), (110), (113), (024), (116), (018), (214) and (300), respectively.[34] These peaks match well with the standard diffraction pattern of α-Fe_2O_3 (hematite) according to JCPDS card no. 33-0664, confirming the successful formation of crystalline hematite nanoparticles. Hematite possesses a rhombohedral crystal structure with space group *R*-3*c*. The mean crystallite size was calculated employing the Debye–Scherrer equation to assess the structural properties of the synthesized NPs.

$$D = K\lambda/\beta \cos\theta$$

Here, D represents the mean crystallite dimension, K signifies the Scherrer constant which has a fixed value of 0.9, λ represents the value of wavelengths associated with a particular X-ray that was used, β denotes the full width at half maximum (FWHM) of the diffraction peak, and θ corresponds to the Bragg's diffraction angle. The average crystallite size calculated using the Debye–Scherrer equation was found to be approximately 44.01 nm. This value aligns with that established in prior research.[35–37]

The morphology of the HNPs was thoroughly studied using HRTEM analysis, and their morphology is illustrated in Fig. 2. The HRTEM images clearly show different detailed features, as seen in Fig. 2a–d at various magnifications. The HNP mostly possesses a spherical morphology along with different polydisperse forms, as illustrated in Fig. 2c. Calculation of the *d*-space values from the SAED pattern was followed by comparison with the reference data from JCPDS card number 33-0664. This analysis not only validated the results but also confirmed the crystalline nature and lattice plane indexing of the HNPs (Table S1). The planes of the *d* space are depicted in Fig. 2e, providing further insight into the structural characteristics of the HNPs. These particular shapes have well-established sizes with an average diameter of 32.18 nm (Fig. 2f), which is extremely close to the average value attained for the crystalline particle size using XRD. Furthermore, the distance between the two points within the lattice was measured to be 0.24359 nm, which closely reflects the average *d*-space value for plane (020) obtained using XRD analysis.

The elemental compositions of the HNPs were also thoroughly analyzed using the EDAX technique, as shown in Fig. 2g. In the analysis, the key elements identified are Fe, O, C, and Cu. The carbon detected can be attributed to the phytochemical materials incorporated within the HNPs, while the copper grid utilized in the HRTEM analysis was present as the copper for this result. The elemental composition indicates that iron constitutes approximately 44.55% of the HNPs, with oxygen also making up around 36.69%, as clearly seen in Fig. 2g.

Outcomes from the Brunauer–Emmett–Teller (BET) analysis were utilized to determine the average diameter of both the surface and pores of the HNPs as described graphically in Fig. 3. The type IV isotherm with an H3 hysteresis cycle gives a clear indication that HNPs have a mesoporous property. The HNPs have an average surface area approximated at 28 ± 1 m^2 g^{-1}, a value greater than that of commercial Fe_2O_3. Moreover, the large average pore diameter of 17.7 nm supports the HNPs having a mesoporous property.[38,39] The appearance of a hysteresis cycle along with a large surface area and large pore diameter can support and improve their potential as a catalyst for various environmental remediation applications.

3.2 Kinetic reduction study of ANC

3.2.1 Catalytic dosage. The dosage or amount of the catalyst is a significant factor in the reduction process. An appropriate dosage of the catalyst must be utilized as it greatly influences the efficiency of the reduction process, dictating the manner in which the molecule is reduced. A perfect balance in

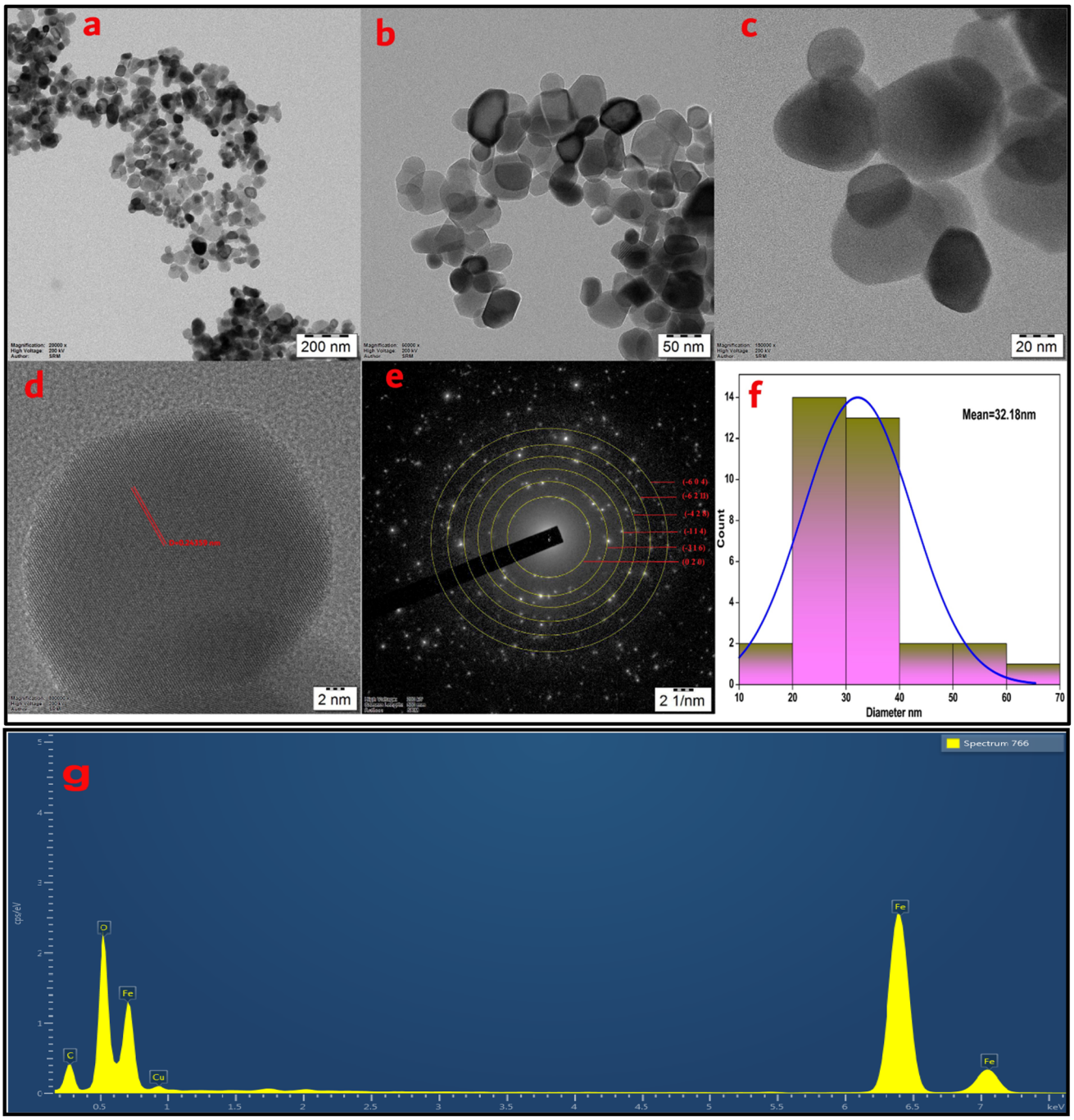

Fig. 2 HRTEM images of HNPs at different magnifications: (a) 200 nm; (b) 50 nm; (c) 20 nm; (d) 2 nm; (e) SAED pattern; (f) particle size distribution histogram; and (g) EDAX analysis of HNPs.

terms of dosage is vital to significantly enhance the reduction process. To determine the reduction for a catalytic dosage of ANC, a reduction study was performed with a 1 M solution of 4-NP. As shown in Fig. 4 and Table 1, the optimal catalytic amount for the reduction of ANC is well defined. The information shown in Table 1 indicates that with a 6.25 mol% catalyst dosage of HNPs, a higher rate of conversation is obtained compared to a 0.0625 mol% or 0.625 mol% catalyst dosage. On the basis of the above data, a constant catalyst dosage of 6.25 mol% is obtained and established as the fixed catalyst dosage for the subsequent reduction kinetics studies.

3.2.2 Reduction of ANC. The systematic reduction of ANC was performed using an optimized catalyst dosage with a fixed characteristic wavelength of ANC. In this work, the time-dependent method (10 min) of UV-vis spectroscopy using a PerkinElmer Lambda 25 instrument was utilized to closely monitor the progression of the reaction. This study compared the reduction of ANC by the standard reducing agent, $NaBH_4$, to

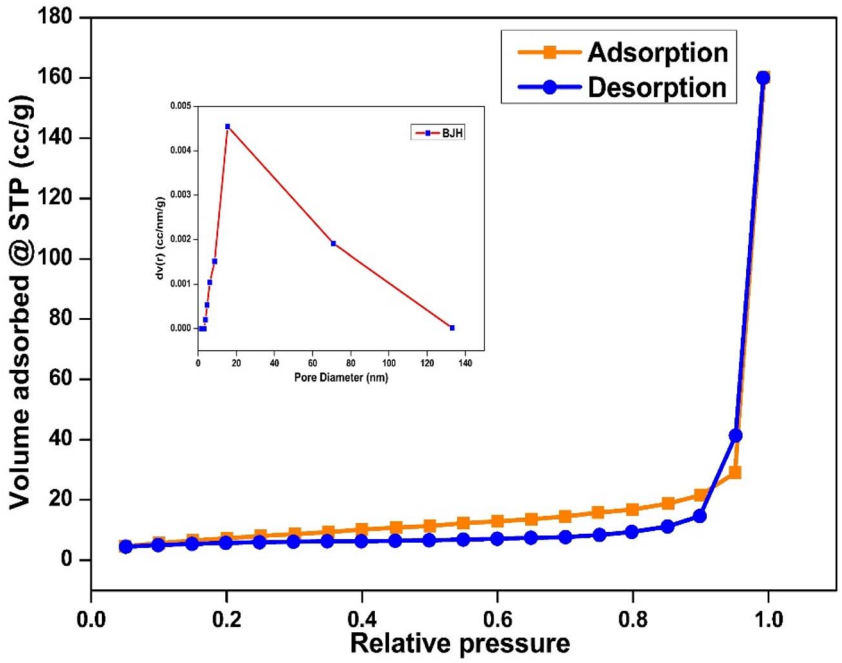

Fig. 3 N_2 adsorption–desorption isotherm of HNPs. (Inset shows BJH pore size distribution curve).

the performance of the green-synthesized HNPs. The reduction of ANC was first conducted with $NaBH_4$ using an optimized dosage of HNP. Approximately 2 mL of the 1 M ANC (2 mmol) compound was placed in a cuvette together with the standard 1 mL of 1 M $NaBH_4$. The reaction was permitted to continue for 10 minutes. Following this, a similar procedure was employed to reduce the ANC using the HNP catalyst. After the 10 min reaction period, the ANC were reduced and successfully synthesized into aromatic amine compounds (AAC). After the reduction process, the loaded HNP catalyst was carefully removed by centrifuging the reaction solution at about 2000 rpm to separate the HNPs as residue. The resulting centrifuged solution contains AAC. The resulting AAC products were meticulously scanned between 200 and 800 nm to identify significant shifts in absorption maxima or the formation of new peaks indicative of amine compounds. The characteristic peak

Table 1 Effect of HNP catalyst dosage (mol%) on the observed K_{ob} and percentage conversion of ANCs to the corresponding AACs under identical reaction conditions. (Conditions: ANC = 2 mmol and temp = 38 °C)

Entry	HNP loading (mol%)	$K_{ob} \times 10^{-3}$ (min^{-1})	Conversion to AAC %
1	0.0625 mol%	8.8	16.65
2	0.625 mol%	19.01	28.6
3	6.25 mol%	178.98	83.95

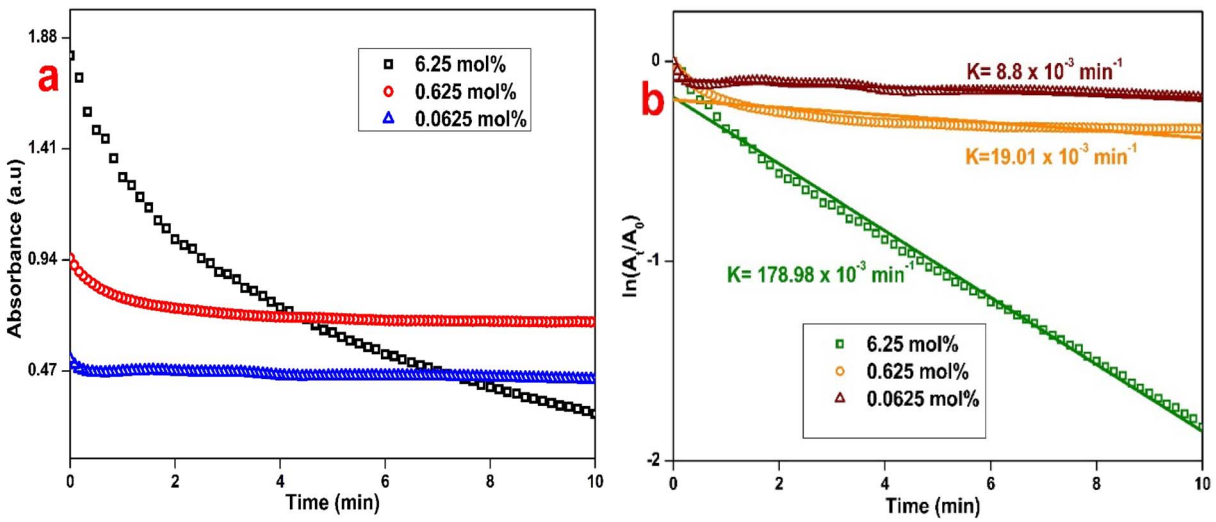

Fig. 4 Catalytic dosage: (a) absorbance *vs.* time and (b) $\ln(A/A_o)$ *vs.* time (conditions: ANC = 2 mmol and temp = 38 °C).

Table 2 UV-vis characteristic absorption peaks of ANCs and their corresponding AACs, showing the fixed monitoring wavelengths used for reduction studies and the spectral shifts confirming nitro-to-amine conversion[a]

ANC	λ_{max} (nm)	Monitoring λ (nm)	AAC	λ_{max} (nm)
4-NP	316 (1.64)	316	4-AP	290 (0.34)
4-NA	231 (0.22) 413 (0.35)	413	1,4-DAB	224 (0.17)
2-NB	247 (5.88)	247	2-AB	220 (0.38), 277 (1.6)
2,4-DNA	264 (1.63) 336 (4.67)	336	1,2,4 TAB	221 (0.18), 266 (0.21), 335 (0.20)

[a] (): Absorbance value. 4-AP: 4-aminophenol. 1,4-DAB: 1,4-diaminobenzene. 2-AB: 2-aminobenzaldehyde. 1,2,4 TAB: 1,2,4 triamine benzene.

values for both the ANC and the resultant reduced AAC are summarized in Table 2 and illustrated in Fig. S1. Upon the addition of $NaBH_4$, only nitrophenolate formation was observed,[40,41] with no conversion to the corresponding amine, as clearly shown in Fig. S13.

3.2.3 Kinetic study. In this study, pseudo first-order kinetics were employed to investigate the reduction ANC using HNPs.[42] The observed rate constant (K_{ob}) for the reduction process was determined using the following equation.

$$\ln(A_t/A_0) = K_{ob}t$$

In this equation, A_t and A_0 are the absorbance measured at defined time points and the initial absorbance, respectively. The constants K_{ob} and C refer to the observed kinetic rate constant and the intercept derived from the regression plot,

Table 3 Kinetic reduction data for ANCs by HNPs

ANC	$K_{ob} \times 10^{-3}$ (min^{-1}) $NaBH_4$	$K_{ob} \times 10^{-3}$ (min^{-1}) HNPs	[a]TON	$NaBH_4$ $T_{1/2}$ min	HNPs $T_{1/2}$ min	% Of conversion [b]$NaBH_4$	% Of conversion HNPs
4-NP	173	179	13.4	4.01	3.87	80.6	84.0
4-NA	26.0	256	15.1	26.7	2.71	28.0	94.4
2-NB	ND	576	14.2	ND	0.97	27.3	88.4
2,4-DNA	ND	18.4	1.8	ND	37.7	28.1	11.4

[a] ND: Not determined. TON (Turn over number) = Yield%/mol% of catalyst. [b] Led to formation of nitrophenolate only.

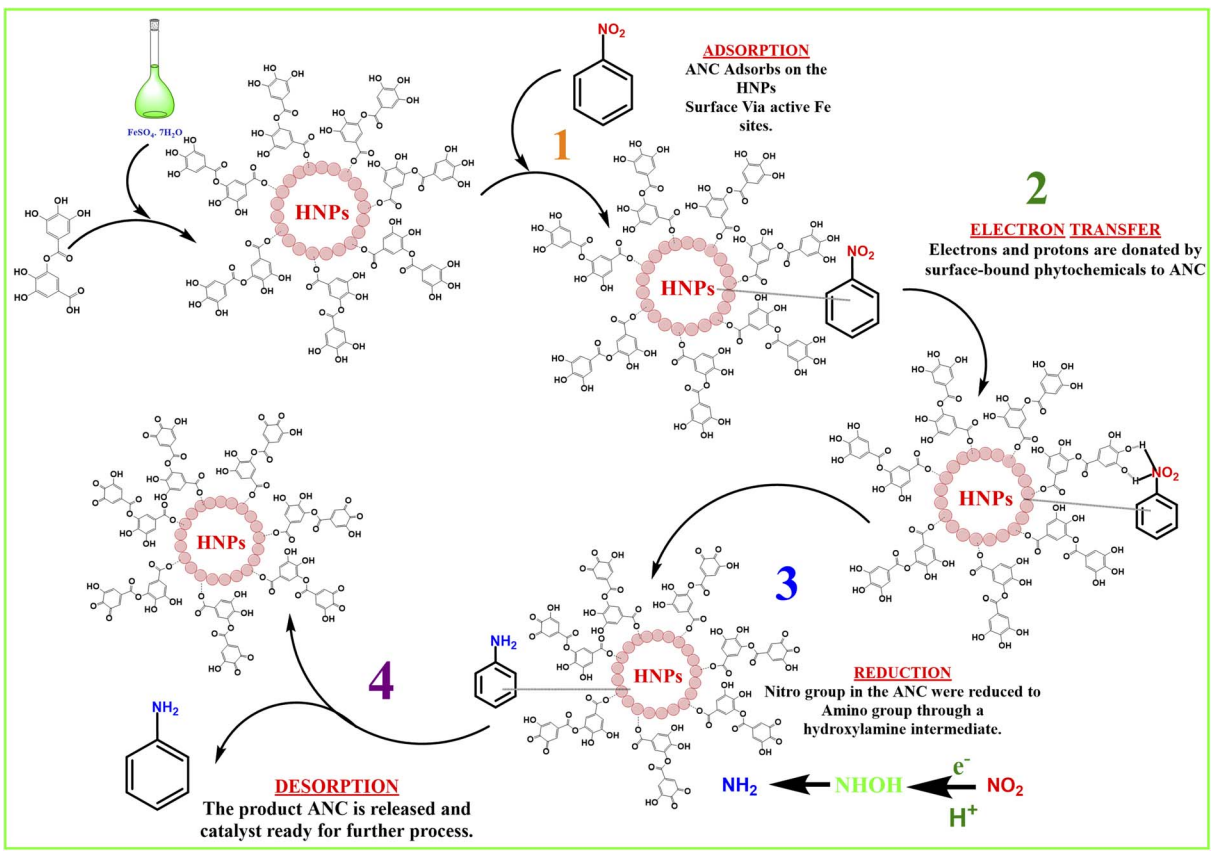

Fig. 5 Schematic of the reduction mechanism of ANC by phytochemical-assisted HNPs.

respectively. The value of K_{ob} was obtained from the slope of the corresponding graph of ln (A_t/A_0) against t. A comparative analysis was conducted to evaluate the reduction efficiency of ANC using HNPs in comparison to standard $NaBH_4$. The rate constants and detailed kinetic data for the reduction processes are summarized in Table 3. The kinetic analysis showed that HNPs exhibit a higher reduction efficiency for mono-nitro compounds than for di-nitro compounds. Though the reduction rate with HNPs for di-nitro compounds is relatively slower, it has a higher rate constant than that of $NaBH_4$.

It is important to note that, for 4-NP reducibility, the rate observed with HNPs is comparable to that of $NaBH_4$ but with a significantly higher conversion rate. Additionally, for 2-NB reducibility, HNPs possess a higher maximum rate constant and improved conversion percentage when compared to $NaBH_4$. The 4-NA compound showed the highest rate constant and conversion rate among the standard $NaBH_4$ and other ANCs evaluated in this reduction study. The rate constants for the reduction of these ANCs using both HNPs and $NaBH_4$ are clearly illustrated in Fig. S2, S3 and S5–12.

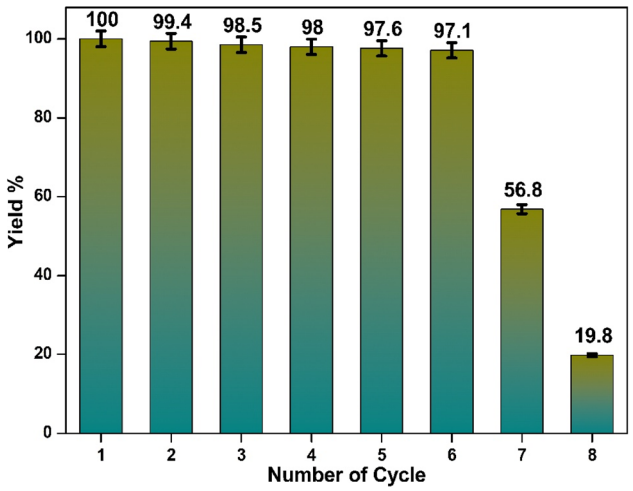

Fig. 6 Recyclability of the HNP catalyst for the reduction of 4-NP, where the first cycle is taken as 100% activity.

3.2.4 Proposed reduction mechanism. The catalytic reduction activity of the HNPs on the ANCs follows the Langmuir–Hinshelwood mechanism, as illustrated in Fig. 5, without any external hydrogen source.[43–45] Initially, the ANC molecules are adsorbed onto the active surface sites of the HNPs, which mostly consist of Fe^{3+} ions along with trace amount of Fe^{2+} ions.[46,47] Subsequently, an active hydrogen atom and electron[48] were transferred to the NO_2 group from phytocompounds such as tannins (polyphenolic compounds), which were bound to the surface of the HNPs during the fabrication process.[49] During the transfer process of electron and hydrogen to the O- atom in the nitro group were assist by the Fe^{3+} ions in the HNPs. This results in the formation of hydroxylamine from the nitro group. At this stage, an additional H-atom is attached to the nitrogen atom, creating a quaternary nitrogen atom. This is subsequently followed by the elimination of a water molecule, creating the AAC[50–53] molecule, and the catalyst is ready for reuse with the formation of Fe^{3+} ions.

3.2.5 Catalyst recyclability. The recyclability of the HNPs was analyzed in consideration of the reduction studies conducted. In this context, the recyclability efficiency of HNPs was checked during the reduction reaction with 4-NP for a total of eight cycles. After concluding each reduction reaction, the particles were centrifuged at around 2000 rpm for the separation of the particles from the reaction mixture. The particles were then rinsed thoroughly with TDW and dehydrated at 80 °C in a convection oven for complete removal of particles before the next cycle. It is evident, as depicted in Fig. 6 and S4, that the catalyst retained high activity for the first six cycles, after which a gradual decrease in activity was observed. It is important to realize, however, that as the cycle count went beyond six, there was also a decline in the reducing capacity of the materials, which fell to ~20% for the HNPs. This decline resulted from

Table 4 Literature comparison of the reported catalysts for the reduction of ANCs, highlighting catalyst loading, reaction temperature, conversion time, and apparent pseudo-first-order rate constants (K_{ob}) under different reaction conditions[a]

Catalyst	Substrate	Reductant	Catalyst loading (mg)	Temp. (°C)	$K_{ob} \times 10^{-3}$ (min^{-1})	Conversion time (min)	Reference
Ag NPs	4-NP	$NaBH_4$	NM	38	91.2	35	55
Fe_3O_4@Ag	4-NP	$NaBH_4$	0.4	38	66	6	56
Au/BIF-20	4-NP	KBH_4	5	38	140	16	57
Ag/P-4A-zeolite	4-NP	NM	NM	NM	64	NM	58
Ag-PNA-BIS-2	4-NP	$NaBH_4$	280	38	90	180	59
C–Ni/350	4-NP	$NaBH_4$	0.5	38	106.8	20	60
Fe_3O_4–Ni/C	4-NP	$NaBH_4$	0.5	38	49.8	20	60
C–Ni/700	4-NP	$NaBH_4$	0.5	38	19.8	20	60
Fe_3O_4@guar gum/Ag nanocomposite	4-NP	$NaBH_4$	3	38	69	60	61
Au NPs	4-NAI	$NaBH_4$	590	38	162.5	60	54
Se-p-C_3N_4/Cu (80)	4-NP	$NaBH_4$	80	75	51.3	60	62
Ag NPs	4-NP	$NaBH_4$	NM	NM	159.7	15	63
ZnO NPs	4-MNB	$NaBH_4$	10	25	26.8	120	64
HNPs	4-NP	Nil	20	38	179	10	Present work

[a] NM: Not mentioned. 4-MNB: 4-methoxynitrobenzene. 4-NAI: 4-nitroanisole.

organic compound formation, oxidation of NPs in air, or loss of catalyst material during recycling.[54]

$$\%\ \text{of recycle ability} = \frac{\%\ \text{of conversion ability of } n \text{ time}}{\%\ \text{of conversion ability of 1 cycle}} \times 100$$

3.2.6 Catalytic activity comparison. In this context, the catalytic performance of HNPs was rigorously assessed and compared with those of a range of other catalysts, as listed in Table 4 below. The table present the conversion rates for 4-NP to 4-AP. According to the obtained results, the HNPs exhibit a competitive catalytic performance compared with previously reported catalysts. This superiority can be credited to reasons such as their striking catalytic activity, stimuli-responsive nature, excellent reusability, and exceptional stability.

4 Conclusion

In summary, hematite nanoparticles were successfully synthesized using an environmentally friendly green synthesis approach employing the *S. grandiflora* leaf extract. The plant extract served as both a reducing and stabilizing agent during nanoparticle formation. The synthesized nanoparticles were thoroughly characterized using UV-vis spectroscopy, FTIR, XRD, HRTEM, EDAX, and BET analyses. The prepared HNPs exhibited excellent catalytic performance in the reduction of various aromatic nitro compounds, following pseudo-first-order reaction kinetics. Additionally, the catalyst demonstrated good stability and recyclability over multiple reaction cycles. The results indicate that green-synthesized HNPs have significant potential as efficient nanocatalysts for environmental remediation applications.

Author contributions

Johnson: writing – original draft, software, methodology, investigation, formal analysis, data curation. Monikadevi: visualization. Rama: project administration, formal analysis. Jothika: validation, investigation. Sivakami: supervision. Roopan: writing – review & editing. Muthu: visualization, validation, supervision, resources, methodology, conceptualization, writing – review & editing.

Conflicts of interest

The authors declare that they have no competing financial or non-financial interests.

Data availability

All experimental data supporting the findings of this study are included within the article and supplementary information (SI). Supplementary information is available. See DOI: https://doi.org/10.1039/d5ra09934j.

Acknowledgements

This research was financially supported by the University Grants Commission (UGC) of the Government of India. JPJ received the Junior Research Fellowship (JRF) awarded under the National Eligibility Test (NET) (Beneficiary Code: BTNTI00556463). The authors express their gratitude to the Department of Chemistry and the Sir C. V. Raman Central Instrumentation Facility at Manonmaniam Sundaranar University, Tirunelveli, India, for their assistance in conducting this research and for the FTIR analysis conducted at SIC-SFRC, Sivakasi. We are also thank the SRM Institute of Science and Technology in Kattankulathur, Chengalpattu District, Tamil Nadu, for their assistance in XRD analysis and TEM with SAED characterization. This research work was also financially supported by the Anusandhan National Research Foundation (ANRF) under the Partnerships for Accelerated Innovation and Research (PAIR) project, Government of India, sanction order ANRF/PAIR/2025/000011/PAIR-B.

References

1 A. Haleem, A. Shafiq, S.-Q. Chen and M. Nazar, *Molecules*, 2023, **28**, 1081.
2 J. Tiwari, P. Tarale, S. Sivanesan and A. Bafana, *Environ. Sci. Pollut. Res.*, 2019, **26**, 28650–28667.
3 P. Kovacic and R. Somanathan, *J. Appl. Toxicol.*, 2014, **34**, 810–824.
4 C. Fernandez-Lopez, R. Posada-Baquero and J.-J. Ortega-Calvo, *Sci. Total Environ.*, 2022, **843**, 157007.
5 M. Orlandi, D. Brenna, R. Harms, S. Jost and M. Benaglia, *Org. Process Res. Dev.*, 2016, **22**, 430–445.
6 A. P. Bhat and P. R. Gogate, *J. Hazard. Mater.*, 2021, **403**, 123657.
7 M. Bilal, A. R. Bagheri, P. Bhatt and S. Chen, *J. Environ. Manage.*, 2021, **291**, 112685.
8 U. Habib, F. Ahmad, M. Awais, N. Naz, M. Aslam, M. Urooj, A. Moqeem, H. Tahseen, A. Waqar and M. Sajid, *J. Chem. Environ.*, 2023, **2**, 14–53.
9 P. Niyirora and P. Cyganowski, *Chem. Eur J.*, 2025, **31**, e202500281.
10 A. Kachore, E. Bala, V. Aggarwal, H. Singh, M. H. A. Suleiman, M. Selvaraj and P. K. Verma, *J. Ind. Eng. Chem.*, 2025, **146**, 494–505.
11 M. Arif, F. Tahir, T. Hussain, S. Alrokayan and T. Akhter, *RSC Adv.*, 2025, **15**, 8580–8593.
12 A. R. Patel, I. Patel and S. Banerjee, *Curr. Org. Chem.*, 2024, **28**, 375–389.
13 N. R. Habib, E. Asedegbega-Nieto, A. M. Taddesse and I. Diaz, *Dalton Trans.*, 2021, **50**, 10340–10353.
14 D. Wang and D. Astruc, *Chem. Soc. Rev.*, 2017, **46**, 816–854.
15 D. Formenti, F. Ferretti, F. K. Scharnagl and M. Beller, *Chem. Rev.*, 2018, **119**, 2611–2680.
16 A. M. E. Shafey, *Green Process. Synth.*, 2020, **9**, 304–339.
17 T. Ahmad, R. Phul and H. Khan, *Curr. Org. Chem.*, 2019, **23**, 994–1004.

18 V. Bahadur, A. S. Dehade, D. Das, P. Kamath, S. Pal, B. Manjunath and P. P. Mukhopadhyay, *RSC Mechanochem.*, 2025, **2**, 802–808.
19 D. Wei and C. Darcel, *Chem. Rev.*, 2018, **119**, 2550–2610.
20 P. Rama, V. Thangapushbam, S. Sivakami, M. Jothika, P. Mariselvi, R. Sundaram and K. Muthu, *J. Indian Chem. Soc.*, 2024, **101**, 101142.
21 E. P. Mukhokosi, E. Mushebo, S. Nassejje, N. L. Botha, D. Velauthapillai and M. Maaza, *Sci. Rep.*, 2025, **15**, 19837.
22 A. Rufus, N. Sreeju and D. Philip, *RSC Adv.*, 2016, **6**, 94206–94217.
23 S. M. Nagasundari, K. Murugan, P. Jeyakumar and K. Muthu, *Phosphorus, Sulfur Silicon Relat. Elem.*, 2022, **197**, 254–262.
24 S. Ying, Z. Guan, P. C. Ofoegbu, P. Clubb, C. Rico, F. He and J. Hong, *Environ. Technol. Innovat.*, 2022, **26**, 102336.
25 D. S. Chaudhari, R. P. Upadhyay, G. Y. Shinde, M. B. Gawande, J. Filip, R. S. Varma and R. Zbořil, *Green Chem.*, 2024, **26**, 7579–7655.
26 F. Kurul, B. Doruk and S. N. Topkaya, *Discov. chem.*, 2025, **2**, 68.
27 V. Thangapushbam, P. Rama, S. Sivakami, M. Jothika, K. Muthu, A. I. Almansour, N. Arumugam and K. Perumal, *Heliyon*, 2024, **10**(8), e29457.
28 S. M. Nagasundari, K. Muthu, K. Kaviyarasu, D. A. Al Farraj and R. M. Alkufeidy, *Surf. Interfaces*, 2021, **23**, 100931.
29 J. P. Jesudasson, S. Mangalanagasundari, V. Thangapushbam, R. Perumal, B. Petchimuthu, K. Subramanian, V. Velu, S. Nagaraj, N. Arumugam, A. I. Almansour, M. Santhamoorthy and K. Muthu, *J. Mol. Struct.*, 2025, **1348**, 143481.
30 S. Rajeshkumar, S. V. Kumar, A. Ramaiah, H. Agarwal, T. Lakshmi and S. M. Roopan, *Enzym. Microb. Technol.*, 2018, **117**, 91–95.
31 A. A. Qureshi, S. Javed, H. M. A. Javed, M. Jamshaid, U. Ali and M. A. Akram, *Nanomaterials*, 2022, **12**, 1635.
32 V. Parthasarathy, J. Selvi, P. Senthil Kumar, R. Anbarasan and S. Mahalakshmi, *Polym. Bull.*, 2021, **78**, 2191–2210.
33 X. Wei, R. Liang, M. Jing and X. Huang, *Mater. Technol.*, 2024, **39**, 2334515.
34 A. Lassoued, B. Dkhil, A. Gadri and S. Ammar, *Results Phys.*, 2017, **7**, 3007–3015.
35 M. Sarani, M. Barani, S. Darijani, M. Adeli-Sardou, F. Aghabozorgi and A. Sardashti-Birjandi, *Inorg. Chem. Commun.*, 2024, **170**, 113236.
36 H. M. Asoufi, T. M. Al-Antary and A. M. Awwad, *Environ. Nanotechnol. Monit. Manage.*, 2018, **9**, 107–111.
37 M. F. Al-Hakkani, G. A. Gouda and S. H. Hassan, *Heliyon*, 2021, **7**(1), e05806.
38 R. Vinayagam, S. Pai, T. Varadavenkatesan, M. K. Narasimhan, S. Narayanasamy and R. Selvaraj, *Surf. Interfaces*, 2020, **20**, 100618.
39 L. Upadhyay, S. Dhanapandian, S. Suthakaran, B. Yadav, K. K. Kar, D. Kumar and J. Arikrishnan, *J. Mater. Sci.: Mater. Electron.*, 2025, **36**, 136.
40 K. Zhang, J. M. Suh, J.-W. Choi, H. W. Jang, M. Shokouhimehr and R. S. Varma, *ACS Omega*, 2019, **4**, 483–495.
41 B. Akilandaeaswari and K. Muthu, *J. Taiwan Inst. Chem. Eng.*, 2021, **127**, 292–301.
42 M. Dinesh, S. M. Roopan and C. I. Selvaraj, *J. Photochem. Photobiol. B Biol.*, 2016, **161**, 273–278.
43 S. Chandrappa, K. Vinaya, T. Ramakrishnappa and K. Rangappa, *Synlett*, 2010, **2010**, 3019–3022.
44 K. Ramadas and N. Srinivasan, *Synth. Commun.*, 1992, **22**, 3189–3195.
45 D. Desai, S. Swami, S. Dabhade and M. Ghagare, *Synth. Commun.*, 2001, **31**, 1249–1251.
46 P. R. S. Baabu, H. K. Kumar, M. B. Gumpu, J. Babu K, A. J. Kulandaisamy and J. B. B. Rayappan, *Materials*, 2022, **16**, 59.
47 H. Liu, Y. Wei and Y. Sun, *J. Mol. Catal. Chem.*, 2005, **226**, 135–140.
48 K. Muthu, S. Rini, S. M. Nagasundari and B. Akilandaeaswari, *Inorg. Nano-Met. Chem.*, 2021, **51**, 579–589.
49 K. G. Lakhani, R. Hamid, E. Motamedi and G. Marviya, *Front. Nanotechnol.*, 2025, **7**, 1545413.
50 S. El-Hout, S. El-Sheikh, H. M. Hassan, F. A. Harraz, I. Ibrahim and E. El-Sharkawy, *Appl. Catal., A*, 2015, **503**, 176–185.
51 F. Luan, L. Xie, J. Li and Q. Zhou, *Chemosphere*, 2013, **91**, 1035–1041.
52 K. J. Datta, A. K. Rathi, M. B. Gawande, V. Ranc, G. Zoppellaro, R. S. Varma and R. Zboril, *ChemCatChem*, 2016, **8**, 2351–2355.
53 Y. Orooji, B. Tanhaei, A. Ayati, S. H. Tabrizi, M. Alizadeh, F. F. Bamoharram, F. Karimi, S. Salmanpour, J. Rouhi and S. Afshar, *Chemosphere*, 2021, **281**, 130795.
54 Z. Zhao, D. Wu, D. Lv, X. Zhang, L. Chen and B. Zhang, *Int. J. Biol. Macromol.*, 2024, **270**, 132250.
55 J. Singh, N. Kaur and M. Rawat, *Micro & Nano Lett.*, 2018, **13**, 1600–1603.
56 G. Sharma and P. Jeevanandam, *Eur. J. Inorg. Chem.*, 2013, **2013**, 6126–6136.
57 H.-X. Zhang, M. Liu, X. Bu and J. Zhang, *Sci. Rep.*, 2014, **4**, 3923.
58 F. Collins, A. Rozhkovskaya, J. G. Outram and G. J. Millar, *Microporous Mesoporous Mater.*, 2020, **291**, 109667.
59 R. Begum, Z. H. Farooqi, A. H. Aboo, E. Ahmed, A. Sharif and J. Xiao, *J. Hazard. Mater.*, 2019, **377**, 399–408.
60 L. Ding, L. Yang, J. Xu, J. Zheng and M. Zhang, *Inorg. Chem.*, 2021, **60**, 8880–8889.
61 J. Su, P. Zhang, X. Han, C. Sui, A. F. El-kott, A. S. Alshehri, M. A. AlShehri, K. Morsy and S. Negm, *J. Organomet. Chem.*, 2024, **1015**, 123225.
62 N. S. Nouri, F. Nemati and M. S. Mirhosseyni, *J. Mol. Struct.*, 2024, **1316**, 139057.
63 P. Bhati, R. Tiwari, S. Kothari, K. Ray, N. P. Lamba, Y. Kumar, R. Binsuwaidan, M. Saeed, S. Obaidur and S. C. Srivastava, *Front. Microbiol.*, 2025, **16**, 1584066.
64 A. B. Ali, A. A. Mohammed, N. S. S. Singh, M. A. Rusho, A. Abilkasimov, B. Saydullaev, L. Safarova, A. Smerat, A. Ali and S. Islam, *J. Organomet. Chem.*, 2025, 123817.